Surface & Coatings Technology 325 (2017) 650–655

Contents lists available at ScienceDirect

Surface & Coatings Technology

journal homepage: www.elsevier.com/locate/surfcoat

Hardening of Al thin films by Ti—C doping

Felipe S. Alencastro [a], Emanuel Santos Jr [a,b], Martin E. Mendoza [c,d], Joyce R. Araújo [c], Sergio Suarez [e], Bráulio S. Archanjo [c], Renata A. Simão [a,*]

[a] Dept. of Metallurgical and Materials Engineering, COPPE, Universidade Federal do Rio de Janeiro (UFRJ), Rio de Janeiro, RJ, Brazil
[b] Centro Universitário de Volta Redonda (UniFOA), Volta Redonda, RJ, Brazil
[c] Materials Metrology Division, Instituto Nacional de Metrologia, Qualidade e Tecnologia (Inmetro), Xerém, RJ, Brazil
[d] Facultad de Ingenieria Mecánica y Ciencias de la Producción, Escuela Superior Politécnica del Litoral, Guayaquil, Ecuador
[e] Centro Atómico Bariloche, Consejo Nacional de Investigaciones Científicas y Técnicas (CONICET), Bariloche, Argentina

ARTICLE INFO

Article history:
Received 8 February 2017
Revised 7 July 2017
Accepted in revised form 10 July 2017
Available online 10 July 2017

Keywords:
Magnetron sputtering
Titanium carbide
Aluminum
Nanocomposite films
Hardness
Nanoindentation

ABSTRACT

Amorphous aluminum alloys have been evaluated as suitable thin films for protective coatings. Magnetron sputtering deposition may provide the necessary conditions for preparing such alloys due to its far-from-equilibrium deposition conditions. In this work, Al-Ti-C nanocomposite films were deposited by magnetron sputtering technique using TiC and Al targets. The produced films are mainly composed of Al nanocrystallites embedded into an amorphous matrix. Films effective hardness varied in the 6.4–8.2 GPa range, while their elastic modulus ranged from 109 up to 134 GPa. The higher the TiC/Al target power ratio, the harder the film. Topographic atomic force microscopy (AFM) images showed that films are mainly constituted by unevenly dispersed grains. Also, the dark phase angle fraction calculation derived from the phase angle contrast AFM images could be correlated with the deposited Al–Ti–C films hardness measured by nanoindentation tests; the higher the surface dark phase angle fraction, the harder the Al–Ti–C films.

1. Introduction

Although aluminum films present potential use for different applications [1–3] they usually show low hardness (H) and elastic modulus (E) [3], being susceptible to scratches and plastic (permanent) deformation. Different methods have been developed for improving mechanical properties. As an example, a 90% increase in aluminum hardness has been achieved by ion bombardment with oxygen [4]. Carbon ion bombardment led to an increase in hardness from 275 MPa to approximately 760 MPa using doses of 10^{18} ions/cm^2. This increase was caused by the formation of aluminum carbide [5].

Recently, ceramic compounds (TiC, SiC) incorporated into Al films are being investigated in order to combine their mechanical properties with those from Al, such as enhanced reflectivity and corrosion resistance [6,7]. Ceramic-based films may be used to increase the surface resistance of tools and mechanical components [7,8], being useful for a number of industrial applications as a wide range of distinct coatings can be produced depending on their thicknesses, crystalline structures and chemical compositions [9,10]. TiC films can have high internal compressive stresses, which reduce film-substrate adhesion and increase film brittleness [11]. Binary aluminum alloys produced by magnetron sputtering with the addition of niobium, molybdenum and tantalum [12,13] were amorphous in most of the aluminum content range, but crystalline alloys could be obtained as well as crystalline-amorphous mixed films.

Aluminum was also combined with TiC or a-C for achieving superior coating properties [6,14–16]. Even so, few studies have been published about the preparation and characterization of Al–Ti–C nanocomposite films containing an amorphous matrix [6,7,16–18]. Pang et al. [7] have deposited Ti–Al–C films using TiAl and graphite targets and showed that, by increasing the substrate bias, the sp^3/sp^2 carbon hybridization ratio in the films becomes steadily lower with increasing Al content. As a consequence, the films hardness decreased from 37 to 22 GPa. On the other hand, the Al addition into sputtered TiC–Al films improved their oxidation resistance [6,17].

The present study is focused on the relation between structure, deposition parameters and nano-mechanical properties of aluminum films with the addition of TiC produced by double magnetron

* Corresponding author at: Universidade Federal do Rio de Janeiro, Dep. de Engenharia Metalúrgica e de Materiais, Caixa Postal 68505, CEP 21941-972 Rio de Janeiro, Brazil.
E-mail address: renata@metalmat.ufrj.br (R.A. Simão).

http://dx.doi.org/10.1016/j.surfcoat.2017.07.023
0257-8972/

sputtering. Transmission electron microscopy (TEM) images showed a fine dispersion of nanocrystals embedded in an amorphous matrix. Phase angle contrast AFM images were correlated to the films hardness assessed by nanoindentation tests.

2. Experimental

2.1. Samples preparation

Films were deposited by double magnetron sputtering on glass slides (25 × 25 mm) and silicon (111) wafer (20 × 20 mm) substrates using pure-Al (99.99%, ∅ = 3″, K.J. Lesker, USA) and TiC targets (99.5%, ∅ = 3″, K.J. Lesker, USA). Aluminum was deposited using a *DC* power supply while TiC via RF sputtering at 13.56 MHz. Film composition and structure were varied by changing the power applied to the different targets. Prior to depositions, substrates were ultrasonically degreased in isopropyl alcohol for 15 min. All depositions were carried out at 0.1 Pa working pressure, 10 sccm Ar flow and 85.0 mm substrate-target distance. Neither bias voltages nor heating were applied to the substrates. Deposition time was set to 90 min for all conditions. Thus, coatings containing different Ti–C/Al ratios and thicknesses were produced. Thickness values for all samples are shown on Table 1.

The substrates were fixed on a rotating disc, which alternately immersed them into the plasma of each sputtering target (TiC and pure-Al). Under the rotating disc, a 2-hole plate was placed to ensure that the substrate would be exposed to the plasma only when it was just above the target. The disc rotating speed was kept constant at 60 rpm, so that less than one atomic layer of each constituent (Ti–C or Al) would be deposited at every cycle.

2.2. Samples characterization

Films thicknesses were measured by contact profilometry using a Dektak IIA profilometer. Since the silicon wafer is smoother than the glass substrate, measurements were performed on films deposited on Si wafers. Transmission electron microscopy (TEM) images were obtained using a probe corrected FEI Titan 80–300 microscope operating at 300 kV. TEM samples were prepared by the lift out technique using a focused ion beam (FIB) - FEI Nova Novalab 600 instrument.

Surface chemical composition of the films was evaluated by X-ray photoelectron spectroscopy (XPS; Omicron Nanotecnology). The XPS analyses were performed in an ultra-high vacuum medium using a monochromatic Al Kα X-ray source. Argon ion flux was employed to sputter the surface for depth profile measurements, with energy of 3.5 keV, sample current of 4 μA, 4 × 4 mm rastered area, incidence angle of 45°. Peak analysis was performed after subtraction of a Shirley background using Gaussian–Lorenzian peak shapes obtained from the Casa XPS software package. The signal of C 1 s located at 285 eV was selected for energy calibration. Sample composition was also determined by Rutherford Backscattering (RBS) at the 1.7 MV Bariloche Tandem Accelerator [19] with 2 MeV alpha particles and using the SIMNRA code [20].

The films surface morphologies were analyzed by atomic force microscopy (AFM) using a NanoWizard I (JPK Instruments) microscope. Both topographic and phase angle contrast images (1.0 × 1.0 μm) were obtained at room temperature. Nanoworld NCSTR silicon cantilevers (with integrated tip) with 7.4 N/m spring constant and 160 kHz resonance frequency were used in tapping mode. Besides the topographic images, phase angle contrast ones were obtained and treated using the Gwyddion 2.26 software [21] to evaluate the phase angle dispersion on the surface, which was obtained by the fraction of the harder area formed on the surface.

Hardness (*H*) and elastic modulus (*E*) of the resulting films were assessed by instrumented indentation tests using a Nanoindenter G200 equipment (MTS/Agilent) following the Oliver-Pharr method [22]. A Berkovich-type diamond indenter was employed. Such measurements were carried out on the films deposited on the glass substrates. A total of 25 indents were performed on each sample under successive load cycles of 0.2, 0.4 and 0.8 mN. A fused-silica sample with known properties (H = 9.5 GPa, E = 73.0 GPa) was used for the tip area calibration. Poisson's ratio of 0.25 was used to calculations.

Table 1
Thicknesses of the produced Ti–Al–C films, according to the power applied on each target. (Mean value ± standard deviation).

Sample	TiC target power (W_{RF})	Al target power (W_{DC})	Thickness (nm)*
80:120	80	120	411 ± 21
80:140	80	140	443 ± 23
80:160	80	160	475 ± 13
100:100	100	100	456 ± 23
100:120	100	120	485 ± 82
100:140	100	140	520 ± 11
100:160	100	160	547 ± 48
120:100	120	100	502 ± 29
120:140	120	140	608 ± 19
140:140	140	140	668 ± 37

* $n = 5$.

3. Results and discussion

Al–Ti–C films were prepared by double magnetron sputtering with different current powers applied to TiC and Al targets. From this point on, the samples are identified in accordance with the power applied to each target (TiC:Al), as shown on Table 1. Fig. 1 displays the applied target powers and measured Al–Ti–C films deposition rates. The latter are more dependent on the TiC power target, as indicated by the arrow therein. It was observed that Al and TiC deposition rates considerably changed when both materials were consecutively deposited in comparison to the isolated deposition at constant flows (not shown).

As expected for both targets, the deposition rate increases with increasing target power. The obtained maximum rate is 7.4 nm/min for the 140:140 sample. Taking into account that deposition time was kept constant (90 min) for all depositions, the Al–Ti–C films are 411–668 nm thick.

According to XPS analysis, the 140:140 sample surface composition is about 21% Al, 1% Ti, 49% C and 30% O. The high oxygen concentration may be resulted from atmospheric contamination. Besides that, the composition changed to 60% Al, 8% Ti, 24% C and 8% O after surface sputtering for 275 min. Similar effects were reported by El Mel et al. [23], where argon bombardment onto an oxygen contaminated carbon

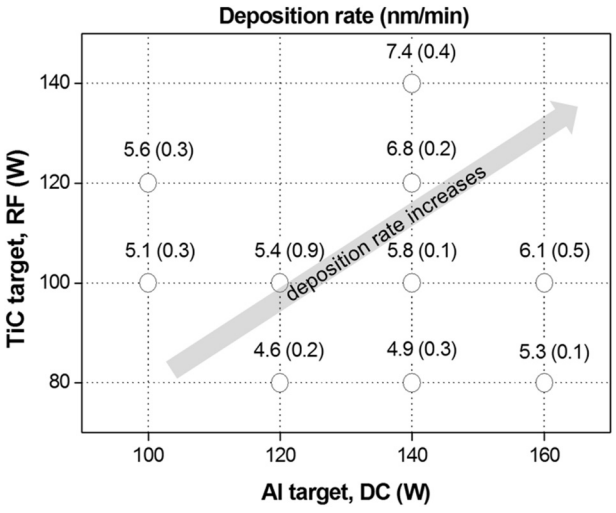

Fig. 1. Deposition rates with respect to the RF/DC powers applied on each target (TiC and Al).

film with TiC particles lead to a preferential sputtering of the matrix, thereby forming a TiC–O rich surface analyzed by XPS. Moreover, the difference between C and Ti contents was reported by Eklund et al. [24] as caused by the shorter mean free path of sputtered titanium atoms when compared to the same parameter for carbon atoms. Notwithstanding, RBS analysis indicates the mean composition of 76% Al, 8% Ti, 15% C and 1% O for the same sample (140:140). Therefore, the films compositions were preferentially evaluated by RBS analysis. Fig. 2 shows the RBS results for analyzed films. Ti:Al content ratio was observed to be dependent on the DC:RF power ratio. In Fig. 3a, a TEM image of sample 140:140, collected in underfocus condition then highlighting mass contrast, shows titanium-rich darker areas (as circled ones). Selected area electron diffraction analysis of the area in Fig. 3a (inset in Fig. 3a) shows a polycrystalline pattern with five rings having *d*-spacing values of 2.35 Å, 2.00 Å, 1.41 Å, 1.22 Å and 1.17 Å, corresponding to Al (111), (200), (220), (311) and (222) planes, respectively.

In Fig. 3b, a high-resolution TEM (HRTEM) image of the same sample shows nanocrystals surrounded by amorphous regions. These nanocrystals have diffraction fringes with *d*-spacing compatible with Al(111). Therefore, it is indicated that this film is composed of Al nanocrystallites (<5 nm) embedded into an amorphous non-homogeneous matrix. In addition, Raman spectroscopy analysis (not shown) indicates no presence of amorphous carbon phase. In fact, it can be assumed that all coatings should present a similar structure, as discussed next.

Fig. 4 shows the AFM topography and phase angle contrast images of 140:140 sample. The surface is smooth with roughness in the nanoscale range (Fig. 4a). Also, phase angle contrast images indicate the presence of a harder phase, shown by the darker areas in Fig. 4b. It can be noticed that the phase angle contrast image presents a straight forward relation to the topography indeed. It is well known that phase angle contrast allows to qualitative assessing the surface local relative stiffness [25,26]. From that, it can be argued that the film morphology is composed of grains, which are stiffer than the matrix and unevenly dispersed on the surface. To quantify the amount of stiffer regions on the surface, phase angle contrast images were segmented using the Gwyddion software and the amount of dark areas analyzed for different films, as illustrated in Fig. 4c. The calculated dark phase angle fractions (%) are displayed in Fig. 5. It can be seen that the dark phase angle fraction increases with increasing the TiC power. Contrarily, the Al power increase led to a reduction of the dark phase angle fraction. Such results are correlated with films hardness and elastic moduli properties, as follows.

Fig. 6 illustrates the typical load versus displacement curves obtained by instrumented indentation technique for two deposited films,

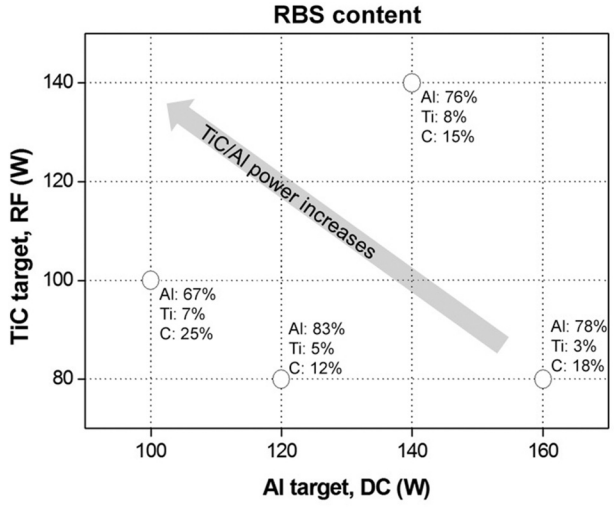

Fig. 2. Films composition measured by RBS spectroscopy. Oxygen content is omitted (<1%). The arrowed line indicates the RF/DC power ratio increase (TiC/Al targets).

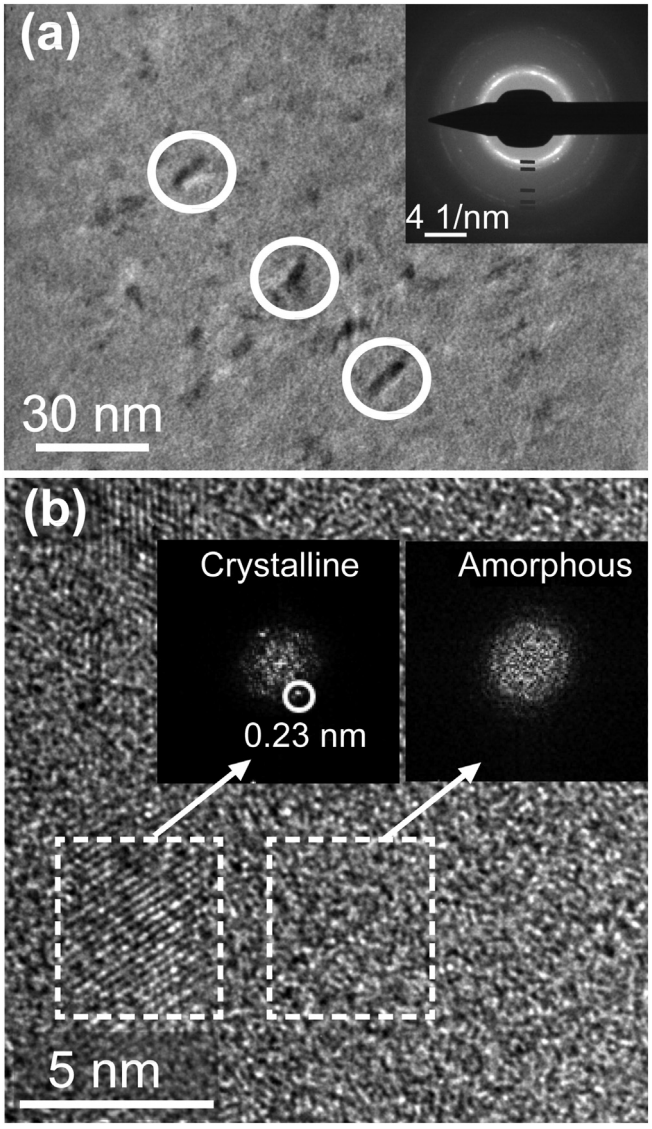

Fig. 3. TEM analyses of Al–Ti–C film (sample 140:140). (a) TEM image, circles show the presence of titanium-rich darker areas. The inset shows a representative electron diffraction pattern. The blue dashes indicate the diffraction rings having d-spacing values of 2.35 Å, 2.00 Å, 1.41 Å 1.22 Å and 1.17 Å, corresponding to Al (111), (200), (220) (311) and (222) planes, respectively. (b) HRTEM showing adjacent crystalline and amorphous regions. The inset shows the fast Furrier transform (FFT) of both regions, the 0.23 nm spaced fringes correspond to Al (111) planes. (For interpretation of the references to colour in this figure legend, the reader is referred to the web version of this article.)

namely 80:160 and 140:140 samples. Both of them presented a similar plastic-elastic deformation behavior for the three applied loads. The absence of pop-ins in the curves is an indication of fracture resistance for the applied loads [22]. Contact depth h_c is determined from the loading-unloading curve, which represents the depth penetration where the material maintains contact with indenter tip, as indicated in Fig. 6. Indeed, the h_c parameter becomes important when evaluating films that possess some degree of elastic deformation, not only the plastic one. Therefore, h_c would be a more accurate parameter for assessing the actual indent depth rather than the maximum penetration h_{max}. Moreover, it can be argued that the highest h_{max} (and h_c) values were obtained for 80:160 sample, being in the 80–85 nm range for the 0.8 mN load. Thus, one can assume that the indenter tip did not reach the substrates, since the thinnest films are about 411 nm thick.

Regarding thin films, it is usual to assume that if the indent depth is larger than 10% of the film thickness, nanoindentation measurements

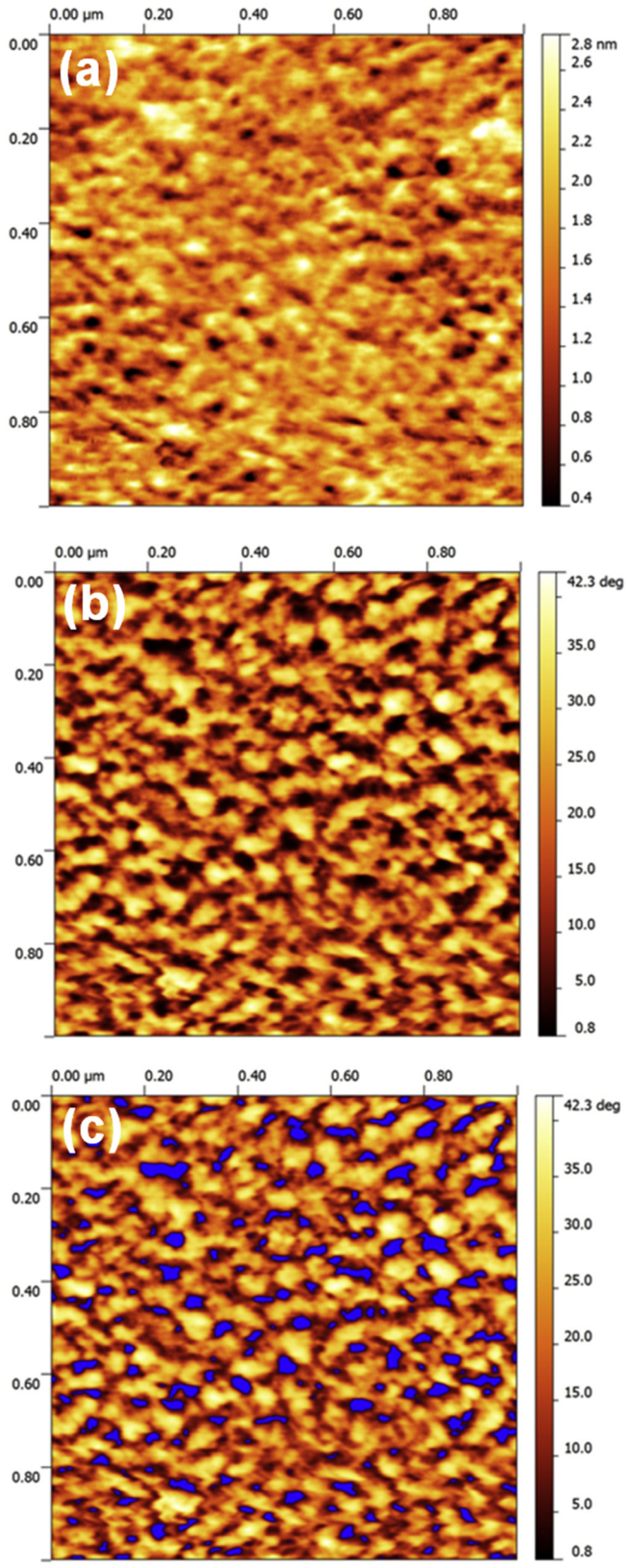

Fig. 4. Atomic force microscopy: (a) topography and (b, c) phase angle contrast images for Al–Ti–C film deposited by double magnetron sputtering (sample 140:140).

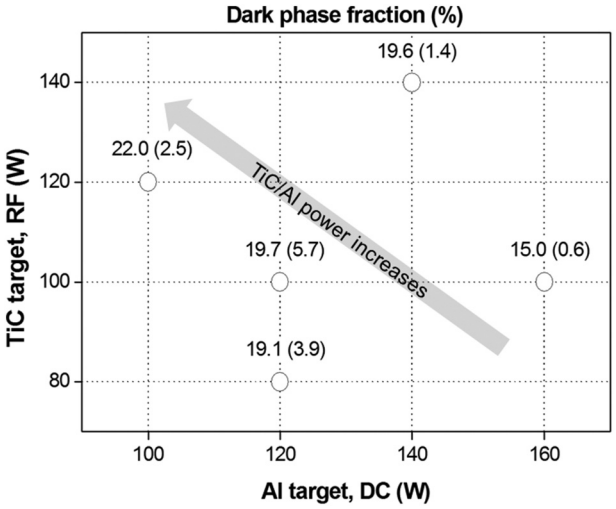

Fig. 5. Dark phase angle fraction (±standard deviation) calculated from AFM phase angle contrast images of the Al–Ti–C films deposited by double magnetron sputtering: TiC (rf power) and Al (DC power) targets. $n = 8$. The arrowed line indicates the RF/DC power ratio increase (TiC/Al targets).

are influenced by the substrate; i.e., hardness is somehow related to film-substrate composite instead of the coating solely [27]. On the other hand, elastic modulus values assessed by indentation through the entire layer region represent actually the coating-substrate composite behavior, since the elastic field under the indenter has a long range, extending into the substrate [27]. Films hardness (H) values calculated from the loading-unloading curves are plotted as a function of the deposition parameters (TiC and Al target power) in Fig. 7. The H values are related to the 0.2 mN load, which led to a maximum penetration depth (hmax) of 35.7 ± 0.9 nm for the sample 80:160. Therefore, the obtained results are mainly referred to the Al–Ti–C films rather than the film-substrate composites.

According to Fig. 7, the hardness tends to increase when the applied power ratio (TiC/Al) is increased. That is, the higher (lower) the power applied to the TiC (Al) target, the harder the film. This statement is, of course, limited to the complexity of the deposition mechanisms involved as well as the parameters used, such as: *DC* and *RF* target powers, Ar flow, working pressure etc. Pure-Al films have been reported to present hardness in the 1.4–2.0 GPa range [3]. On the other hand, TiC–Al films deposited by magnetron sputtering are much harder, having *H* values as high as 25 GPa, depending on the deposition parameters [6,7,18]. Both hardness and elastic modulus increase when the amount of TiC increases [6]. Also, Wilhelmsson et al. [28] have reported Ti_3AlC_2 films 20 GPa hard with and elastic modulus around 260 GPa. In the

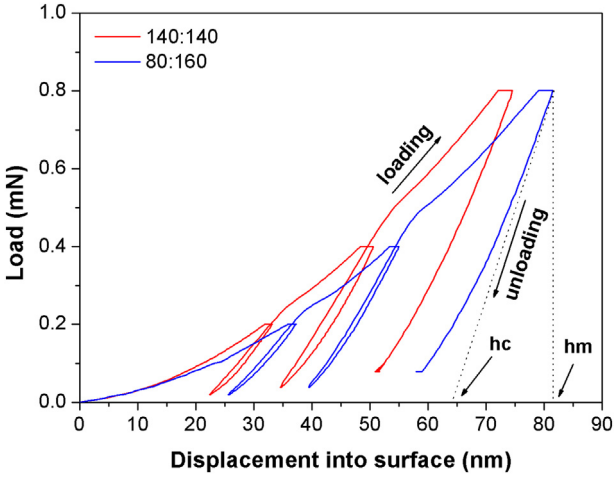

Fig. 6. Typical load versus penetration depth curves from instrumented indentation tests for the Al–Ti–C films deposited by double magnetron sputtering: 140:140 and 80:160 samples. H_{max} is the maximum penetration depth and h_c is the calculated contact depth.

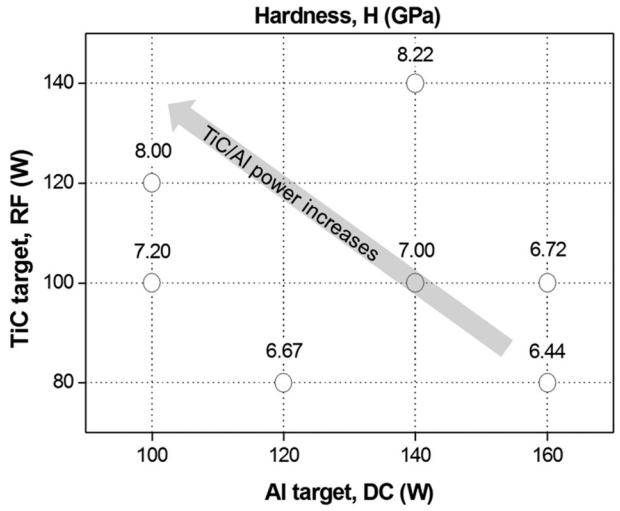

Fig. 7. Hardness (H) values (in GPa) obtained from instrumented indentation tests with respect to the applied TiC and Al target powers for the Al–Ti–C films deposited by double magnetron sputtering. Load = 0.2 mN, n = 25, and maximum standard deviation of about 5%. The arrowed line indicates the RF/DC power ratio increase (TiC/Al targets).

present study, the Al–Ti–C films are considerably harder than pure-Al films, being 6.4–8.2 GPa hard. It is noteworthy that a very similar behavior was obtained by both instrumented indentation tests and AFM analysis. In this way, the dark phase angle fraction can be surely associated with the film hardness – the higher the dark phase angle fraction, the harder the Al–Ti–C film.

Fig. 8 displays the hardness of the Al–Ti–C films with respect to their elastic modulus. The correlation between H and E follows a slight linear relationship. Indeed, E corresponds to the slope of a harmonic interatomic potential, whereas H is more sensitive to the microstructural defects in the network. For amorphous carbon coatings, some studies have argued that the found linear H/E relation comes from the mean compressive strain ($H/2E$) behavior [29,30]. Therefore, this also appears to be the case of amorphous Al–Ti–C films. Furthermore, the H^3/E^2 (or H/E) parameter is also attributed for predicting the wear resistance or the film resistance to permanent deformation [29,31]. In case of Al-doped TiC coatings, the H^3/E^2 ratio increases when the amount of Al is reduced, leading to more wear resistant films [6]. However, this effect does not appear to be the case of Al–Ti–C thin coatings, once the produced films did not present any significant differences among the H^3/E^2 values (~0.06 GPa), regardless of their deposition parameters.

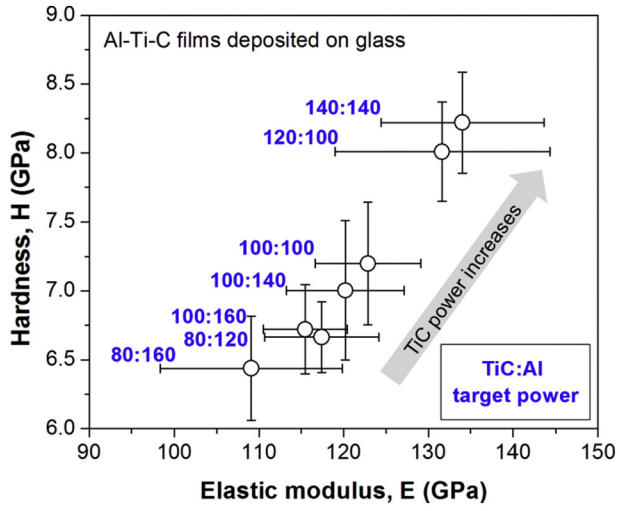

Fig. 8. Hardness (H) versus elastic modulus (E) of the producing Al–Ti–C films measured by instrumented indentation tests; Load = 0.2 mN, n = 25. The arrowed line indicates the RF power increase (TiC target).

The H/E relation is mostly ruled by the *RF* power (TiC target), as also indicated in Fig. 8. It can be observed that the higher the H (and E), the higher the TiC target power. Since the sputtered pure-TiC films are hard (~30 GPa) [6], the Al–Ti–C films deposited at highest *RF* powers (TiC target) may present more ionic bonds, which could be responsible for hardening.

To conclude, once the dark area fractions (AFM analysis) and films hardness (elastic modulus) increased when the TiC deposition power did so, the proposed AFM image analysis can be straightly combined with nano-mechanical properties (hardness and elastic modulus) of the Al–Ti–C films deposited.

4. Conclusions

In this work, Al–Ti–C films were prepared by magnetron sputtering technique. Different *RF* and *DC* powers were applied to TiC and pure-Al targets, respectively. All films presented <10% at. titanium in their compositions. The produced films are constituted by an amorphous matrix containing Al nanocrystallites. Films hardness and elastic modulus were correlated to the deposition parameters. The higher the TiC/Al target power ratio, the harder the films. Likewise, the dark phase angle fraction (derived from phase angle contrast AFM images) increased when the TiC/Al power ratio does so. Therefore, the surface dark phase angle fraction determined by AFM analysis can be correlated with the Al–Ti–C films hardness obtained by nanoindentation tests.

Acknowledgements

This work was partially supported by CNPq (National Council for Scientific and Technological Development) and CAPES (Higher Level Personnel's Improvement Coordination) Brazilian funding agencies.

References

[1] B. Enders, S. Krauß, K. Baba, G.K. Wolf, Ion-beam-assisted deposition of aluminium and aluminium alloy coatings for corrosion protection, Surf. Coat. Technol. 74 (75) (1995) 959–965.
[2] C.J. Wang, J.W. Lee, T.H. Twu, Corrosion behaviors of low carbon steel, SUS310 and Fe–Mn–Al alloy with hot-dipped aluminum coatings in NaCl-induced hot corrosion, Surf. Coat. Technol. 163 (164) (2003) 37–43.
[3] J. Zhang, D. Yang, X. Ou, Microstructures and properties of aluminum film and its effect on corrosion resistance of AZ31B substrate, Trans. Nonferrous Metals Soc. China 18 (2008) s312–s317.
[4] P. Mishra, D. Ghose, The hardness study of oxygen implanted aluminum thin films, Surf. Coat. Technol. 201 (2006) 965–970.
[5] C. Meunier, S. Vives, F. Munnik, G. Berthout, S. Mikhailov, Effect on microstructure and hardness of 1 MeV carbon ion implantation in Al, Co and W, Surf. Coat. Technol. 262 (2015) 191–199.
[6] J. Soldan, J. Musil, P. Zeman, Effect of Al addition on structure and properties of sputtered TiC films, Plasma Process. Polym. 4 (2007) S6–S10.
[7] X. Pang, L. Shi, P. Wang, G. Zhang, W. Liu, Influences of bias voltage on mechanical and tribological properties of Ti–Al–C films synthesized by magnetron sputtering, Surf. Coat. Technol. 203 (2009) 1537–1543.
[8] G. Zhang, B. Li, B. Jiang, F. Yan, D. Chen, Microstructure and tribological properties of TiN, TiC and Ti(C, N) thin films prepared by closed-field unbalanced magnetron sputtering ion plating, Appl. Surf. Sci. 255 (2009) 8788–8793.
[9] D. Chicot, Y. Bénarioua, J. Lesage, Hardness measurements of Ti and TiC multilayers: a model, Thin Solid Films 359 (2000) 228–235.
[10] A. Mani, P. Aubert, F. Mercier, H. Khodja, C. Berthier, P. Houdy, Effects of residual stress on the mechanical and structural properties of TiC thin films grown by RF sputtering, Surf. Coat. Technol. 194 (2005) 190–195.
[11] H. Wang, S. Zhang, Y. Li, D. Sun, Bias effect on microstructure and mechanical properties of magnetron sputtered nanocrystalline titanium carbide thin films, Thin Solid Films 516 (2008) 5419–5423.
[12] T. Car, N. Radić, P. Panjan, M. Čekada, A. Tonejc, Correlation between hardness and stress in Al–(Nb, Mo, Ta) thin films, Thin Solid Films 517 (2009) 4605–4609.
[13] J. Ivkov, K. Salamon, N. Radić, M. Sorić, Thermal stability of Al–Mo thin film alloys, J. Alloys Compd. 646 (2015) 1109–1115.
[14] H. Chaliyawala, G. Gupta, P. Kumar, G. Srinivas, Siju, H. Barshilia, Structural and mechanical properties of reactively sputtered TiAlC nanostructured hard coatings, Surf. Coat. Technol. 276 (2015) 431–439.
[15] S. Zhang, X. Bui, Y. Fu, Magnetron-sputtered nc-TiC/a-C(Al) tough nanocomposite coatings, Thin Solid Films 467 (2004) 261–266.

[16] O. Wilhelmsson, J.-P. Palmquist, E. Lewin, J. Emmerlich, P. Eklund, P.O.Å. Persson, H. Högberg, S. Li, R. Ahuja, O. Eriksson, L. Hultman, U. Jansson, Deposition and characterization of ternary thin films within the Ti–Al–C system by DC magnetron sputtering, J. Cryst. Growth 291 (2006) 290–300.
[17] Q.M. Wang, W. Garkas, A.F. Renteria, C. Leyens, H.W. Lee, K.H. Kim, Oxidation behaviour of Ti–Al–C films composed mainly of a Ti_2AlC phase, Corros. Sci. 53 (2011) 2948–2955.
[18] X. Pang, L. Shi, P. Wang, Y. Xia, W. Liu, Effects of Al incorporation on the mechanical and tribological properties of Ti-doped a-C:H films deposited by magnetron sputtering, Curr. Appl. Phys. 11 (2011) 771–775.
[19] S. Limandri, C. Olivares, L. Rodriguez, G. Bernardi, S. Suárez, PIXE facility at Centro Atómico Bariloche, Nucl. Instrum. Meth. B 318 (2014) 47–50.
[20] M. Mayer, SIMNRA, A simulation program for the analysis of NRA, RBS and ERDA, in: J.L. Duggan, I.L. Morgan (Eds.),Proc. of the 15th ICAARI, AIP Conference Proceedings, 475, 1999, p. 541.
[21] D. Nečas, P. Klapetek, Gwyddion: an open-source software for SPM data analysis, Cent. Eur. J. Phys. 10 (2012) 181–188.
[22] W.C. Oliver, G.M. Pharr, An improved technique for determining hardness and elastic modulus using load and displacement sensing indentation experiments, J. Mater. Res. 7 (1992) 1564–1583.
[23] A. El Mel, B. Angleraud, E. Gautron, A. Granier, P. Tessier, XPS study of the surface composition modification of nc-TiC/C nanocomposite films under in situ argon ion bombardment, Thin Solid Films 519 (2011) 3982–3985.
[24] P. Eklund, M. Beckers, J. Frodelius, H. Högberg, L. Hultman, Magnetron sputtering of Ti_3SiC_2 thin films from a compound target, J. Vac. Sci. Technol. A 25 (2007) 1381–1388.
[25] H. Ahn, S. Chizhik, A. Dubravin, V. Kazachenko, V. Popov, Application of phase contrast imaging atomic force microscopy to tribofilms on DLC coatings, Wear 249 (2001) 617–625.
[26] S. Magonov, V. Elings, M. Whangbo, Phase imaging and stiffness in tapping-mode atomic force microscopy, Surf. Sci. 375 (1997) L385–L391.
[27] R. Saha, W.D. Nix, Effects of the substrate on the determination of thin film mechanical properties by nanoindentation, Acta Mater. 50 (2002) 23–38.
[28] O. Wilhelmsson, J.P. Palmquist, T. Nyberg, U. Jansson, Deposition of Ti_2AlC and Ti_3AlC_2 epitaxial films by magnetron sputtering, Appl. Phys. Lett. 85 (2004) 1066–1068.
[29] A. Leyland, A. Matthews, On the significance of the H/E ratio in wear control: a nanocomposite coating approach to optimised tribological behaviour, Wear 246 (2000) 1–11.
[30] C.A. Charitidis, Nanomechanical and nanotribological properties of carbon-based thin films: a review, Int. J. Refract. Met. Hard Mater. 28 (2010) 51–70.
[31] D. Martínez-Martínez, C. López-Cartes, A. Fernández, J.C. Sánchez-Lopez, Influence of the microstructure on the mechanical and tribological behavior of TiC/a-C nanocomposite coatings, Thin Solid Films 517 (2009) 1662–1671.